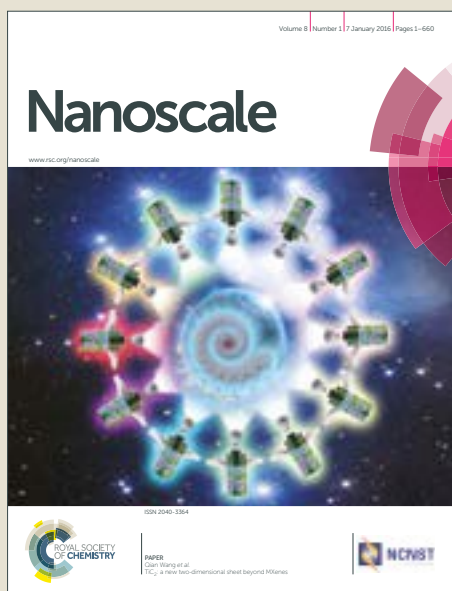


Nanoscale

Accepted Manuscript



This article can be cited before page numbers have been issued, to do this please use: D. Klepac, H. Kostkova, S. Petrova, P. Chytil, T. Etrych, S. Kereïche, I. Raska, D. A. Weitz and S. K. Filippov, *Nanoscale*, 2018, DOI: 10.1039/C7NR09355A.



This is an Accepted Manuscript, which has been through the Royal Society of Chemistry peer review process and has been accepted for publication.

Accepted Manuscripts are published online shortly after acceptance, before technical editing, formatting and proof reading. Using this free service, authors can make their results available to the community, in citable form, before we publish the edited article. We will replace this Accepted Manuscript with the edited and formatted Advance Article as soon as it is available.

You can find more information about Accepted Manuscripts in the [author guidelines](#).

Please note that technical editing may introduce minor changes to the text and/or graphics, which may alter content. The journal's standard [Terms & Conditions](#) and the ethical guidelines, outlined in our [author and reviewer resource centre](#), still apply. In no event shall the Royal Society of Chemistry be held responsible for any errors or omissions in this Accepted Manuscript or any consequences arising from the use of any information it contains.



Nanoscale

ARTICLE

Interaction of Spin-Labeled HPMA-based Nanoparticles with Human Blood Plasma Proteins – Introduction of protein-corona free polymer nanomedicines

Damir Klepac,^{*,a} Hana Kostková,^a Svetlana Petrova,^a Petr Chytil,^a Tomáš Etrych,^a Sami Kereiche,^b Ivan Raška,^b David A. Weitz,^c and Sergey K. Filippov^{*,a}

Received 00th January 20xx,
Accepted 00th January 20xx

DOI: 10.1039/x0xx00000x

www.rsc.org/

In this paper, we revised current understanding of the protein corona that is created on the surface of the nanoparticles in blood plasma after intravenous injection. We have focused on nanoparticles that have a proven therapeutic outcome. These nanoparticles are based on two types of biocompatible amphiphilic copolymers based on *N*-(2-hydroxypropyl)methacrylamide (HPMA): a block copolymer poly(ϵ -caprolactone) (PCL)-*b*-poly(HPMA) and statistical HPMA copolymer bearing cholesterol moieties, which have been tested both *in vitro* and *in vivo*. We studied the interaction of nanoparticles with blood plasma and selected blood plasma proteins by electron paramagnetic resonance (EPR), isothermal titration calorimetry, dynamic light scattering, and cryo transmission electron microscopy. The copolymers were labeled with TEMPO radicals at the end of hydrophobic PCL or along the hydrophilic HPMA chains to monitor changes in polymer chain dynamics caused by protein adsorption. By EPR and other methods, we were able to probe specific interactions between nanoparticles and blood proteins, specifically low- and high-density lipoproteins, immunoglobulin G, human serum albumin (HSA), and human plasma. It was found that individual proteins and plasma have very low binding affinity to nanoparticles. We observed no hard corona around HPMA-based nanoparticles; with the exception of HSA the proteins showed no detectable binding to the nanoparticles. Our study confirms that a classical “hard corona-soft corona” paradigm is not valid for all types of nanoparticles and each system has unique protein corona that is determined by the nature of NP material.

Introduction

For the delivery of drugs to a specific cell or organ, it is important to overcome pharmacokinetic limitations associated with conventional drug formulations.¹ It was proven that polymeric nanoparticles (NPs), i.e. self-assembled micelles, composed of amphiphilic copolymers could be successfully used as carriers for drug delivery.² These colloidal polymeric systems provide control over the drug pharmacokinetics and biodistribution and at the same time improve the stability of the drug while it is delivered by the blood to the therapeutic place of action.^{3,4} In addition, NPs can be designed to deliver many types of drugs by combining polymers of different structure, chemical composition, hydrophilicity and charge.³ It is well known that there are more than 3700 proteins in

blood and some of them bind to the surfaces of NPs immediately after injection of the materials into a bloodstream forming the so-called “protein corona”.^{5–15} This corona is the biological identity of a nanoparticle, as it is what the cell ‘sees’ and interacts with.¹⁶ The interaction of drug delivery systems with blood proteins is therefore regarded as the most important issue that determines the nanoparticle stability, biodistribution, efficacy and toxicity.^{7,17,18}

Nowadays, it is generally accepted that the protein corona has two shells – soft and hard coronas.¹⁹ The hard corona consists of tightly bound proteins with high affinity. These proteins can’t be removed from the NPs surface even by strong agitation such as extensive centrifugation and washing. The soft corona is composed of proteins with lower affinity. It is believed that proteins in the soft corona are in dynamic equilibrium with environment. It were Vroman and Adams who first discovered that the composition of proteins adsorbed on a surface changes with time.²⁰ More abundant plasma proteins like human serum albumin (HSA) are substituted with less abundant but more active proteins such as immunoglobulin G (IgG) and fibrinogens over time. Although it is not proven yet experimentally, the Vroman effect should be valid for NPs as well. Nevertheless, a few reports were published on nanoparticles with low or protein-free corona.^{21,22} It was also established earlier that the

^a Institute of Macromolecular Chemistry of the Czech Academy of Sciences, Heyrovsky Sq. 2, 162 06 Prague 6, Czech Republic.

^b Institute of Biology and Medical Genetics, First Faculty of Medicine, Charles University, Albertov 4, 128 01 Prague 2, Czech Republic.

^c Gordon McKay Laboratory, Harvard University, Oxford Street Cambridge, MA 02138, USA.

Electronic Supplementary Information (ESI) available: EPR simulation parameters, additional DLS data and Cryo-TEM images, description of the basic characterization techniques. See DOI: 10.1039/x0xx00000x

ARTICLE

Journal Name

absorption of proteins could be controlled by the composition of copolymer.^{23,24}

The real drawback of the vast majority NPs whose interactions with blood plasma has already been reported in literature is that they are not suitable for drug delivery. In this paper, we want to examine the protein corona of therapeutic NPs in blood plasma after intravenous injection.

Despite the broad range of methodologies used to study NP-protein interaction, including: UV-Vis,²⁵ fluorescence spectroscopy,²⁵ capillary electrophoresis,²⁶ nanoparticle tracking analysis (NTA) method combined with field flow fractionation (FFF) and multi-angle light scattering (MALS),²⁷ dynamic light scattering (DLS),^{28–31} isothermal titration calorimetry (ITC) and gel electrophoresis (SDS-PAGE),⁶ liquid chromatography (LC-MS/MS),³² none of the mentioned techniques can directly probe the dynamics of polymer chains in the NP hydrophobic core and hydrophilic shell during interaction with proteins. Such dynamical changes could be a good marker of the protein presence on NP surface.

Electron paramagnetic resonance (EPR) spectroscopy however is a powerful technique for studying the motion of nitroxyl radicals covalently attached to a molecule of interest. This technique is known as a “spin-labeling” and it has been successfully applied to study the dynamics of various polymer systems, proteins and lipids.^{33,34} Li *et al.* have used EPR technique to study the dynamic changes within telodendrimer-based NPs during interaction with blood proteins.³⁵ They found that the proteins and lipoproteins from blood plasma may influence the stability of NPs and rapidly destroy their structure. Additionally, they proposed that the stability of investigated NPs could be improved by introducing disulfide cross-links in the core of NPs.³⁵

Recently, we have developed a new type of radical containing nanoparticle (RNP) based on poly[N-(2-hydroxypropyl)methacrylamide] (poly(HPMA)) as the hydrophilic block and a hydrophobic poly(ϵ -caprolactone) (PCL) block. These RNPs could potentially find applications as drug delivery systems and for the treatment of oxidative stress injuries.³⁶ The nitroxyl radicals located in a hydrophobic core of the NPs can be used as spin labels for EPR studies. Another type of nanoparticle containing amphiphilic HPMA copolymer bearing cholesterol as the hydrophobic moiety located along the hydrophilic polymer chain was developed previously.^{37,38} Its conjugates with the anti-cancer drug doxorubicin, bound to the polymer carrier by a pH-sensitive bond, showed prolonged blood circulation, enhanced tumor uptake, controlled drug release in tumor tissue/cells and superior anticancer activity *in vivo*.

For EPR studies the NPs were covalently labeled with 2,2,6,6-tetramethylpiperidine-1-oxyl (TEMPO) radicals located at the end of the PCL block or randomly distributed along the hydrophilic HPMA copolymer chain.

The present study aims to investigate the influence of blood plasma and various plasma components on chain dynamics in RNP containing the label in the hydrophobic PCL core or hydrophilic HPMA copolymer shell and verify the validity of the

classical “hard corona – soft corona” approach for HPMA copolymer-based NPs.

Experimental

Materials

Acetic acid, 1-aminopropan-2-ol, methacryloyl chloride, 6-aminohexanoic acid, methyl 6-aminohexanoate hydrochloride, hydrazine hydrate, cholesterol, *N,N*-diisopropylethylamine (DIPEA), 4,5-dihydrothiazole-2-thiol, dimethylacetamide (DMA), dimethyl sulfoxide (DMSO), ϵ -caprolactone (ϵ -CL, 99%), 2,2'-azobis(2-methylpropionitrile) (AIBN, 98%), 4-cyano-4-(thiobenzoylthio)pentanoic acid (CTA, >97%), 4-(dimethylamino)pyridine (DMAP, 99%), *N,N*'-dicyclohexylcarbodiimide (DCC, 99%), *m*-chloroperbenzoic acid (*m*CPBA, $\leq 77\%$) and tin(II) bis(2-ethylhexanoate) (Sn(Oct)₂, 95%, 0.06 M solution in toluene), 4-hydroxy-2,2,6,6-tetramethylpiperidine (TEMPO, 98%), 4-amino-TEMPO and 4-oxo-TEMPO (TEMPONE) were purchased from Sigma-Aldrich. High-density lipoprotein (HDL) and low-density lipoprotein (LDL) were purchased from Lee Biosolutions, Inc. (Maryland Heights, USA). Human plasma was obtained from the Military University Hospital in Prague from healthy donors. Human serum albumin (HSA), bovine serum albumin (BSA), immunoglobulin G (IgG), sodium dodecyl sulfate (SDS) and all other chemicals were purchased from Sigma-Aldrich.

Synthesis of monomers

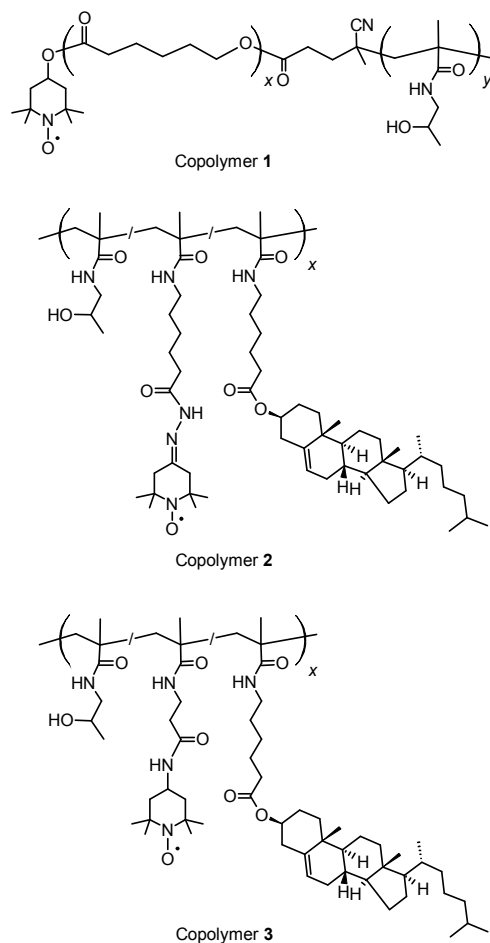
N-(2-hydroxypropyl)methacrylamide (HPMA) was synthesized according to ref.³⁹ Cholest-5en-3 β -yl 6-methacrylamido hexanoate (MA-Ahx-Chol) was prepared as described in ref.³⁷ 3-(3-Methacrylamidopropanoyl)thiazolidine-2-thione (MA- β Ala-TT) was prepared as described in ref.⁴⁰ 6-methacrylamido hexanoyl hydrazine (MA-Ahx-NHNH₂) was synthesized as described in ref.⁴¹

Synthesis of spin-labeled PCL-*b*-poly(HPMA) diblock copolymer

A detailed synthetic procedure of TEMPO-PCL-*b*-poly(HPMA) (copolymer **1**) is described in our previous publication.³⁶ Briefly, α -2,2,6,6-tetramethylpiperidin- ω -hydroxy-PCL prepolymer (α -TEMP-PCL) was obtained *via* ring-opening polymerization (ROP) of ϵ -CL initiated by 4-hydroxy-2,2,6,6-tetramethylpiperidine. In the second step, the PCL-CTA macromolecular chain transfer agent (PCL macroCTA agent) was prepared from α -TEMP-PCL in high yield by carbodiimide chemistry (DCC) method. The resulting PCL macroCTA agent was applied in the third reaction step under reversible addition-fragmentation chain transfer (RAFT) polymerization conditions to supply the PCL-*b*-poly(HPMA) diblock copolymers. In the last step, oxidation by *m*-chloroperbenzoic acid of 2,2,6,6-tetramethylpiperidin groups in the composition of the diblock copolymers afforded the corresponding stable TEMPO radicals. The copolymer **1** was used for the preparation of RNP containing the label in the hydrophobic core (RNP-C).

Synthesis of spin-labeled HPMA copolymers bearing cholesterol

Two types of random HPMA copolymers differing in the spacer length between the spin probe and polymer carrier chain were synthesized.



Scheme 1 Schematic structures of copolymers 1 - 3.

Polymer poly(HPMA-*co*-MA-Ahx-Chol-*co*-MA-Ahx-TEMPONE) (copolymer 2) bearing cholesterol and TEMPONE was synthesized by two step synthesis: Firstly, the terpolymer

poly(HPMA-*co*-MA-Ahx-Chol-*co*-MA-Ahx-NHNH₂) was prepared by free radical polymerization of HPMA, MA-Ahx-Chol and MA-Ahx-NHNH₂ in methanol using AIBN as initiator and purified according to ref.³⁷ Afterwards TEMPONE was bound to the polymer carrier *via* a hydrazone bond with following procedure: 340 mg of polymer poly(HPMA-*co*-MA-Ahx-Chol-*co*-MA-Ahx-NHNH₂) and 3.4 mg of TEMPONE were dissolved in 3.3 mL of methanol and 132 μ L of acetic acid was added into the stirred solution. After 24 h-reaction at 25 $^{\circ}$ C the polymer conjugate was purified from low molecular impurities by gel filtration (Sephadex LH-20, solvent methanol) and isolated by precipitation into ethyl acetate, filtered and dried to constant weight. The yield was 295.6 mg (86.9%). The copolymer 2 was used for the preparation of RNP containing the label in the hydrophilic shell bound by longer spacer (RNP-SI).

Polymer carrier poly(HPMA-*co*-MA-Ahx-Chol-*co*-MA- β Ala-TEMPO) (copolymer 3) bearing cholesterol and 4-amino-TEMPO attached *via* amide bond was prepared by a two-step synthesis: Firstly, the terpolymer of HPMA, MA-Ahx-Chol and MA- β Ala-TT (poly(HPMA-*co*-MA-Ahx-Chol-*co*-MA- β Ala-TT)) was prepared by free radical polymerization in DMSO using AIBN as initiator (AIBN (2 wt.%); monomers (18 wt.%); molar ratio HPMA : MA-Ahx-Chol : MA- β Ala-TT 93:2:5). The resulting polymer was isolated by precipitation into the mixture of acetone:diethylether 2:1, dissolved in methanol and reprecipitated into acetone, washed with diethylether, filtered and dried to constant weight. Then 4-amino-TEMPO was bound to the polymer carrier by aminolysis of the polymer thiazoline-2-thione (TT) groups: 59.3 mg of polymer poly(HPMA-*co*-MA-Ahx-Chol-*co*-MA- β Ala-TT) and 2 mg of 4-amino-TEMPO were dissolved in the mixture of 600 μ L DMA and 400 μ L methanol with 30 μ L of DIPEA. The reaction proceeded at 25 $^{\circ}$ C and after 2 h the polymer conjugate was purified from low molecular impurities by gel filtration (Sephadex LH-20, solvent methanol) and isolated by precipitation into ethyl acetate, filtered and dried to constant weight. The yield was 42.1 mg (68.7%). The copolymer 3 was used for the preparation of RNP containing the label in the hydrophilic shell bound by shorter spacer (RNP-Ss).

Table 1 Physico-chemical characteristics of polymer conjugates

Sample	Structure	M_w (g/mol) ^a	D^a	Content of cholesterol (mol %) ^b	Content of probe (mol %) ^c
Copolymer 1	TEMPO-PCL- <i>b</i> -poly(HPMA)	44 000	1.4	N/A	0.50
Copolymer 2	poly(HPMA- <i>co</i> -MA-Ahx-Chol- <i>co</i> -MA-Ahx-TEMPONE)	27 500	2.3	2	0.03
Copolymer 3	poly(HPMA- <i>co</i> -MA-Ahx-Chol- <i>co</i> -MA- β Ala-TEMPO)	25 000	1.6	2	0.02

^a) Molecular weights (M_w) and dispersity (D) were determined by GPC with MALS detection.

^b) The content of cholesterol was determined by ¹H-NMR.

^c) The content of the spin probe was determined by UV-Vis.

Preparation of the nanoparticles

The core-shell RNP were prepared by the nanoprecipitation method.⁴² Copolymers 1 - 3 (20 mg) were dissolved in

dimethylformamide (DMF) (6 mL). The solutions were then injected drop-wise using a syringe (G=26) into phosphate buffer saline (PBS, pH 7.4) (14 mL) while stirring magnetically

ARTICLE

Journal Name

at room temperature. The organic solvent was removed *via* dialysis in PBS during 24 h using a 3-5 kDa molecular weight

cut-off membrane. The final concentration for both types of NPs was 1.0 mg·mL⁻¹.

Characterization techniques

Electron paramagnetic resonance (EPR) spectroscopy

The solution of spin-labeled NPs (1.0 mg·mL⁻¹) was mixed with SDS, HSA, BSA, HDL, LDL, IgG and human plasma. The final concentrations of the proteins were comparable to the levels usually present in human blood (50 mg mL⁻¹ for HSA and BSA, 2 mg mL⁻¹ for HDL and LDL and 10 mg mL⁻¹ for IgG). EPR measurements were performed using a 20-μL capillary on a Bruker ELEXSYS E-540 X-band spectrometer equipped with a Bruker ER 049X microwave bridge and a Bruker ER4131VT variable temperature unit. Spectra were recorded at 37 °C with a sweep width of 100 G, a microwave power output of 6 mW, a modulation frequency of 100 kHz, and a sweep time of 22 minutes to improve the signal-to-noise ratio. The modulation amplitude was optimized to the line width of the spectrum (on the order of 1.0 to 2.0 G).

EPR simulations

The spectra were simulated using the spectral fitting program NLSL, which is based on the stochastic Liouville equation and utilizes the modified Levenberg–Marquardt minimization algorithm to calculate the best fit with experimental spectra.⁴³ The spin label motion was assumed to follow the Brownian diffusion model with an axially symmetric rotational diffusion tensor. The components of the **g** and **A** tensors were determined by analyzing the rigid limit spectra. All spectra were simulated with a single spectral component. The fits were obtained by varying the parallel and perpendicular rotational diffusion coefficients (R_{prp} , R_{ppl}), the diffusion tilt angle (θ_0) and the inhomogeneous line width tensor (W_1). The quality of the fit was determined according to the correlation coefficient r , which was above 0.99 for all fits.

Rotational correlation times (τ_R) were calculated according to Eq. 1⁴³

$$\tau_R = \frac{1}{6^3 \sqrt{R_{\text{prp}}^2 R_{\text{ppl}}}} \quad (1)$$

Dynamic light scattering (DLS)

The DLS measurements were performed using an ALV CGE laser goniometer. The scattered light of a 22-mW HeNe linear polarized laser (632.8 nm) was collected using an ALV 6010 correlator in a broad angle range of 40–150°. The DLS experiments were conducted at body temperature, $T = 37$ °C. Counting times were varied in a range from 100 to 300 s to accumulate an intensity correlation function $g_2(t)$ with a high signal-to-noise ratio. The measured $g_2(t)$ was analyzed using the algorithm REPES (incorporated in the GENDIST program) resulting in a distribution of relaxation times τ , $A(\tau)$. The translational diffusion coefficient D_{tr} was obtained according to the relation:

$$\Gamma = \tau^{-1} = D_{\text{tr}} q^2 \quad (2)$$

where Γ is the relaxation rate, $q = 4\pi n \sin(\theta/2)/\lambda$ is the magnitude of the scattering vector with λ corresponding to the laser wavelength, n is the refractive index of the solvent, and θ is the scattering angle.

The apparent hydrodynamic radius (R_h) of the NPs was calculated from the Stokes–Einstein relation:

$$R_h = \frac{k_B T}{6\pi\eta D_{\text{tr}}} \quad (3)$$

where k_B is the Boltzmann constant, T is the absolute temperature, η is the viscosity of the solvent, and D is the apparent diffusion coefficient of the NPs.

Cryo-Transmission Electron Microscopy (Cryo-TEM)

Cryo-TEM measurements were carried out using a Tecnai G² Sphera 20 electron microscope (FEI Company, Hillsboro, OR, USA) equipped with a Gatan 626 cryo-specimen holder (Gatan, Pleasanton, CA, USA) and a LaB₆ gun. The samples for cryo-TEM were prepared by plunge-freezing.⁴⁴ Briefly, 3 μL of the sample solution was applied to a copper electron microscopy grid covered with a perforated carbon film forming woven-mesh-like openings of different sizes and shapes (the lacey carbon grids #LC-200 Cu, Electron Microscopy Sciences, Hatfield, PA, USA) and then glow discharged for 40 s with 5 mA current. Most of the sample was removed by blotting (Whatman no. 1 filter paper) for approximately 1 s, and the grid was immediately plunged into liquid ethane held at –183 °C. The grid was then transferred without rewarming to the microscope. Images were recorded at the accelerating voltage of 120 kV and with magnifications ranging from 11500× to 50000× using a Gatan UltraScan 1000 slow scan CCD camera in low-dose imaging mode, with the electron dose not exceeding 1500 electrons per nm². The magnifications resulted in final pixel sizes ranging from 1 to 0.2 nm, and the typical value of the applied underfocus ranged from 0.5 to 2.5 μm. The applied blotting conditions resulted in the specimen thicknesses varying between 100 to ca. 300 nm. Brightness and contrast corrections of the acquired images were performed using ImageJ software.

Isothermal titration calorimetry (ITC)

The isothermal titration microcalorimetry experiments were performed using a MicroCal ITC₂₀₀ calorimeter. The experiment was performed with consecutive injections of the protein solution into the measurement cell; the cell contained 280 μL of the polymer solution or water. A protein solution was added to a 40 μL injection syringe, that was also acting as a stirrer. The stirring speed was in a range 500 - 1000 rpm. The injection volume was 2 μL. The time between injections was usually 200 s. The measurements were recorded at 37 °C. The data were analyzed using Microcal Origin software. Experimental value of enthalpy (ΔH) was obtained by integrating the raw data signal, and the integrated molar enthalpy change per injection was

obtained by dividing the experimentally measured enthalpy by the number of moles of the protein added. The final data are the plots of the integrated molar enthalpy change as a function of the total protein concentration in the calorimeter sample cell.

Results and discussion

Behavior of nanoparticles in phosphate buffer saline (PBS)

Spin-labeled NPs bearing the probe in the hydrophobic core (RNP-C) (Fig. 1(a)) were self-assembled from PCL-*b*-poly(HPMA) diblock copolymers labeled with TEMPO radicals at the end of the hydrophobic PCL block (copolymer **1**). After micellization, the TEMPO radicals are located in the hydrophobic core of the NPs and closely follow the dynamics of the PCL chain.³⁶ Two variants of the spin-labeled NPs

bearing the probe in the hydrophilic shell bound by longer (RNP-SI) or shorter spacer (RNP-Ss) (Figs. 1(b) and (c)) were prepared from the corresponding copolymers **2** and **3** with different spacer lengths between the spin probe and polymer carrier. Here, the NPs were labeled with 4-oxo- (RNP-SI) or 4-amino-TEMPO radical (RNP-Ss) randomly distributed along the hydrophilic HPMA copolymer chain. The spacers between the spin label and HPMA copolymer backbone were composed of two or five methylene groups for RNP-Ss or RNP-SI respectively. Although the TEMPONE spin probe was bound by the hydrazone bond, which can be potentially hydrolytically labile, we observed not more than only 6% of the released probe after 24 h at 37 °C in a phosphate buffer of pH 7.4. Thus, the differences in properties of RNP-Ss and RNP-SI described below can be ascribed only to the spacer length.

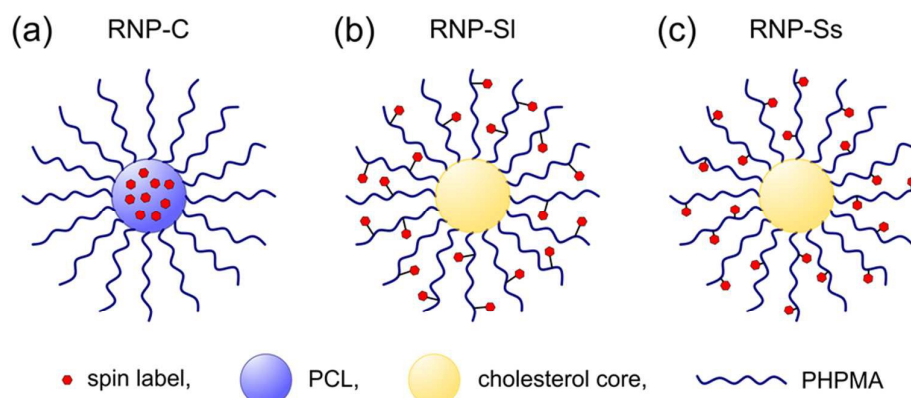


Fig. 1 Schematic representation of spin-labeled NPs containing the spin label (a) in the hydrophobic core (RNP-C), (b) in the hydrophilic shell via longer spacer (RNP-SI) and (c) in the hydrophilic shell via shorter spacer (RNP-Ss).

Dynamic light scattering shows that copolymer **1** forms NPs (RNP-C) in PBS buffer with hydrodynamic radius of ~43 nm with sharp distribution, whereas copolymer **3** self-assembles to form NPs (RNP-Ss) with comparable average radius of 40 nm but a broader distribution (Fig. S1).

To evaluate the ability of the spin label to provide information about the motion of the outer hydrophilic shell of the RNP-Ss or RNP-SI NPs and inner hydrophobic PCL core of RNP-C NPs, we compared the EPR spectra obtained from RNP-C, RNP-Ss and RNP-SI with the spectra of pure TEMPONE radical (Fig. 2).

The characteristic three-line EPR signal of the nitroxyl radical arises due to anisotropic hyperfine interactions between the unpaired electron and nitrogen nucleus.⁴⁵ The narrow EPR lines of almost equal intensities observed for pure TEMPONE are characteristic of very fast motions of the nitroxyl radical in the PBS solution. The EPR spectrum of RNP-SI is very similar to that of pure TEMPONE except for its high field line, which has lower intensity due to the slightly slower (restricted) mobility of the attached nitroxyl radical. However, the EPR spectrum observed for the RNP-Ss is considerably broader (Fig. 2). This broadening of the EPR signal reflects the slower spin

label mobility in RNP-Ss when compared to both TEMPONE and RNP-SI. On the other hand, the EPR spectrum of RNP-C is the broadest one due to the significantly restricted motional freedom of the nitroxyl radical (Fig. 2). This mobility can be quantified by the rotational correlation time, τ_R , which corresponds to the average time during which a radical rotates by one radian. To extract rotational correlation times, we simulated and compared the EPR spectra obtained at 37 °C. The parameters used for the EPR spectral fitting and calculated rotational correlation times are given in Table S1.

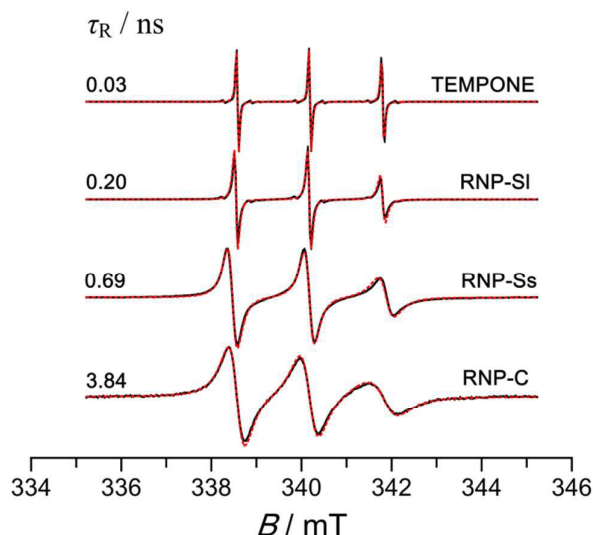


Fig. 2 EPR spectra of pure TEMPONE, RNP-SI, RNP-Ss and RNP-C in PBS buffer at 37 °C. Solid lines represent experimental spectra, and dotted red lines represent simulated spectra.

The simulated EPR spectra of pure TEMPONE, RNP-SI, RNP-Ss and RNP-C in PBS buffer at 37 °C are shown as dotted red lines in Fig. 2. The τ_R values of 0.20 and 0.69 ns obtained for RNP-SI and RNP-Ss, (Fig. 2 dotted red lines, Table S1), confirm that the spin label mobility falls under the fast motional regime (10^{-11} to 10^{-9} s) where the spectral changes are very sensitive to molecular motion.⁴⁶ This is not surprising since the radicals are attached to the outer hydrophilic HPMA copolymer shell of RNP-Ss and RNP-SI through a flexible spacer. The mobility of the spin label in RNP-Ss and RNP-SI is therefore only partially restricted by the HPMA copolymer chains.

τ_R of a spin label attached to a poly(HPMA) backbone with the spacer composed of five methylene groups (RNP-SI) increased more than six times compared to the free TEMPONE radical in PBS solution (from 0.03 ns to 0.20 ns). The longer correlation time indicates the slower dynamics of the spin label after attachment to the polymer backbone. By shortening the spacer length between the spin label and HPMA copolymer chain (RNP-Ss) the correlation time additionally increased to 0.69 ns (23 times compared to the free TEMPONE). The same behavior was observed in proteins where the correlation time of the unbound, free label in aqueous solution increased from ~0.05 ns to 0.80 ns after attachment to a soluble protein fragment.^{47,48} These results are in a good agreement with a previous study by Pilar et. al. who found that the correlation time of the spin label attached to a methacrylamide-based copolymer decreases monotonically with increasing side chain length.⁴⁹

In the case of RNP-C, the calculated τ_R value of 3.84 ns (Fig. 2 dotted red line, Table S1) indicates that the spin label mobility is much more restricted compared to the label in RNP-Ss and RNP-SI. Since the spin labels in RNP-C are attached to the end of the hydrophobic PCL chains, after the self-assembly process they become located in the cores of NPs where their mobility is significantly constrained by the dense hydrophobic environment.

The spin label mobility depends on the flexibility of the spacer that connects it to the backbone and on the motions of the entire macromolecule. To study the dynamics of the HPMA

copolymer chains during interaction with proteins it is necessary to minimize the influence of the internal motions of the nitroxide radical about the chemical bonds of the spacer. Therefore, the NPs with shorter spacer length between the spin label and HPMA polymer carrier (RNP-Ss) were chosen for all subsequent measurements. Rotational correlation time, τ_R can be used as a sensitive parameter to detect the presence of a protein corona on the surface of the NPs.

Effect of sodium dodecyl sulfate on nanoparticles.

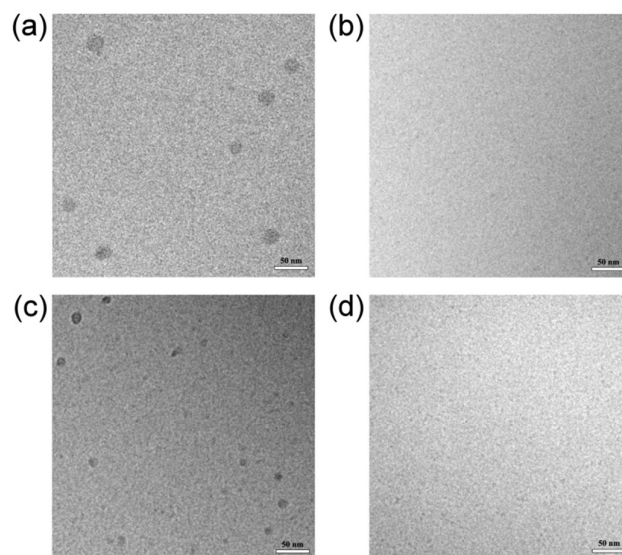


Fig. 3 Cryo-TEM images of (a) RNP-C in PBS buffer, (b) RNP-C in the presence of 2.0 mg mL⁻¹ SDS, (c) RNP-Ss in PBS buffer, (d) RNP-Ss in the presence of 2.0 mg mL⁻¹ SDS.

To verify the sensitivity of the EPR method, we explored the behavior of NPs in the presence of sodium dodecyl sulfate (SDS), a highly effective anionic surfactant commonly used for protein denaturation. SDS molecules attach to proteins mainly by hydrophobic interactions inducing unfolding of the protein tertiary structure. The driving force for this extension arises

from repulsions between the SDS molecules and negatively charged side chains of the protein.⁵⁰ Cryo-TEM and dynamic light scattering (DLS) results (Figs. 3 and S2) clearly show that the structure of RNP-C and RNP-Ss become disrupted in the presence of SDS. For both types of NPs the mode from NPs disappears and two peaks are manifested on a distribution function instead. The slow mode corresponds to the SDS micelles, whereas the second peak could be attributed to the aggregates of SDS and polymeric unimers.

The changes of EPR spectra of RNP-C and RNP-Ss after interaction with SDS are shown in Fig. 4.

The EPR spectrum of RNP-C in SDS (2.0 mg mL^{-1}) shows significantly narrower lines compared to the spectrum in PBS. When the structure of RNP-C is disrupted by SDS, the spin labels which were tightly arranged in the dense hydrophobic core suddenly become exposed to the solution where they have much higher mobility.

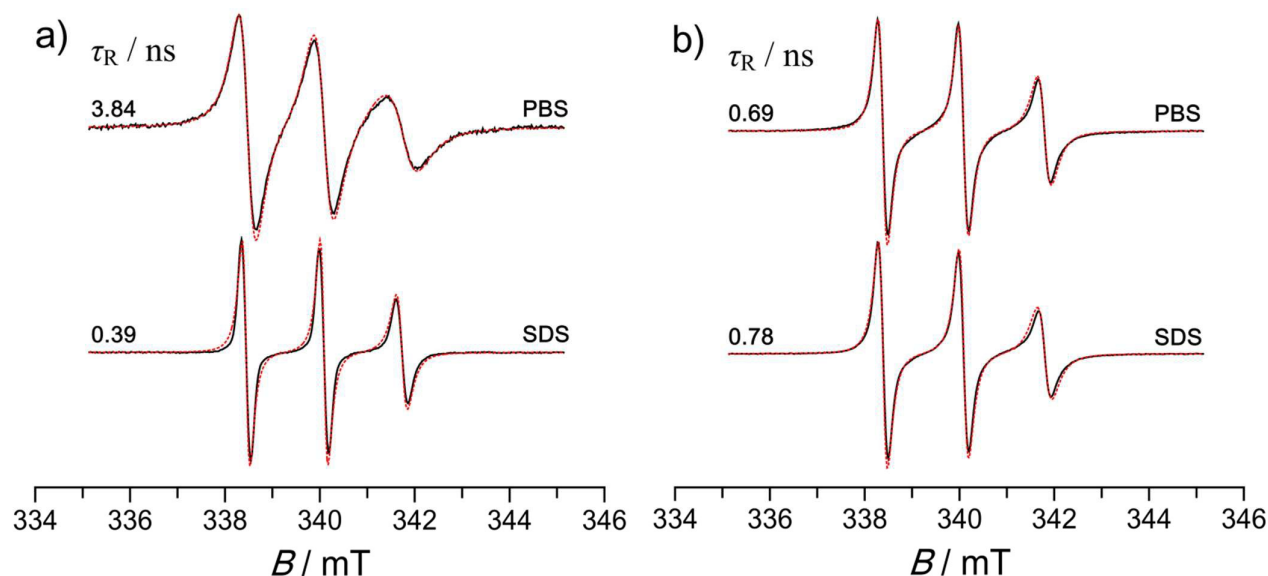


Fig. 4 EPR spectra of (a) RNP-C and (b) RNP-Ss in PBS buffer with and without SDS ($c = 2.0 \text{ mg mL}^{-1}$) at 37°C . Solid lines represent experimental spectra, and dotted red lines represent simulated spectra.

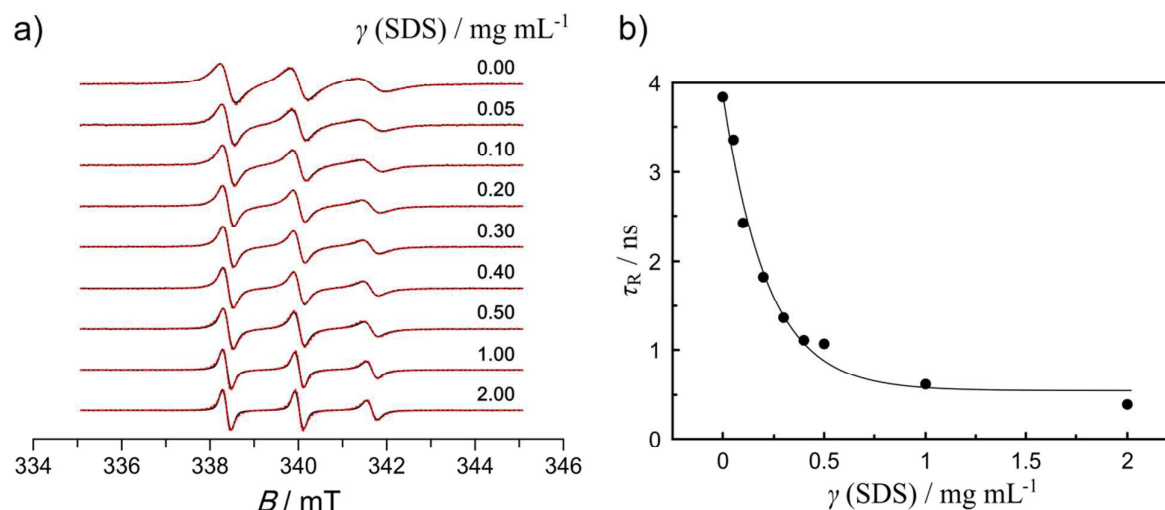


Fig. 5 (a) EPR spectra of pure RNP-C in PBS buffer as a function of SDS concentration at 37°C . Solid lines represent experimental spectra, and dotted red lines represent simulated spectra. (b) The dependence of rotational correlation time as a function of SDS concentration at 37°C , PBS.

Nanoscale

ARTICLE

The calculated τ_R values (Fig. 4(a), Table S2) show that the mobility of spin labels in RNP-C increases by an order of magnitude after interaction with SDS. In the case of RNP-Ss, however, no spectral changes are observed after interaction with SDS and the spectral simulations show only a minor change in the calculated τ_R values (Fig. 4(b), Table S2). Clearly, the disruption of RNP-Ss is not reflected in the EPR spectrum since the spin labels attached on the surface of these NPs already show relatively high mobility even before disintegration. The same effect was observed for non-cross-linked NPs assembled from amphiphilic telodendrimers.³⁵ We also investigated the changes of EPR spectra of RNP-C after treatment with different concentrations of SDS. As shown in Fig. 5(a), the relatively broad spectrum of RNP-C in PBS solution (0.00 mg mL⁻¹ of SDS) gradually narrows with increasing SDS concentration until finally reaching the shape characteristic of fast motion in 2.00 mg mL⁻¹ SDS solution. Simulations reveal that the τ_R values for labels in RNP-C decrease exponentially with increasing SDS concentration (Fig. 5(b), Table S3). Clearly, 1.0 mg mL⁻¹ of SDS is already sufficient

to completely disintegrate the structure of the investigated NPs.

To improve the stability of nanoparticle micelles several techniques such as stereocomplexation,⁵¹ non-covalent interactions^{52,53} and crosslinking^{54–56} have previously been applied. Crosslinked NPs were found to be resistant to SDS disruption.^{35,57,58} Such modifications, however, are not always possible and it is imperative to investigate the stability of prepared NPs in a real blood environment to assess the need for additional stabilization.

Interaction of nanoparticles with proteins

To investigate the interaction of various blood plasma proteins with RNP-C and RNP-Ss the NPs were incubated in HSA, bovine serum albumine (BSA), high-density lipoprotein (LDL), low-density lipoprotein (LDL), IgG and human plasma for 1 h and the EPR spectra were recorded at 37 °C. The concentrations of proteins and lipoproteins were comparable to their typical blood levels.^{59–61} The simulated EPR spectra of RNP-C and RNP-Ss in PBS, plasma and various plasma proteins are shown together with recorded EPR spectra in Fig. 6.

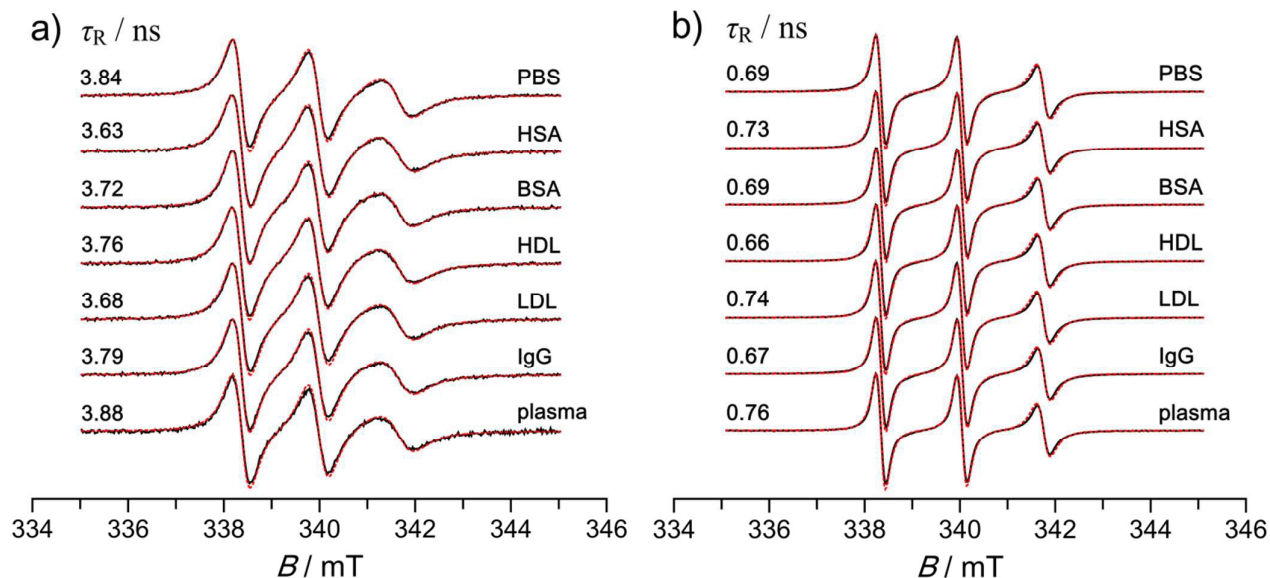


Fig. 6 EPR spectra of (a) RNP-C and (b) RNP-Ss in PBS buffer and in the presence of different proteins at 37 °C, PBS. Solid lines represent experimental spectra, and dotted red lines represent simulated spectra.

Human serum albumin (HSA) is the most abundant protein in plasma and it affects the pharmacokinetics of many drugs due to its extraordinary ligand-binding capacity.⁶² It is generally the first protein that is adsorbed and for this reason it can strongly

influence *in vivo* NP biodistribution.^{5,63} However, the shape of the EPR spectra of RNP-Ss after incubation with HSA and BSA is the same as the spectra in pure PBS (Fig. 6(b)). This observation is also evident by comparing corresponding

rotational correlation times (Fig. 6(b), Table S5). These results indicate that HSA and BSA do not significantly bind to the outer HPMA copolymer shell of RNP-Ss and the protein corona is not formed. Moreover, the τ_R values for RNP-C remain essentially unchanged after incubation with HSA and BSA (Fig. 6(a), Table S4), indicating that serum albumins are not able to penetrate poly(HPMA) shell and enter the PCL core where they could influence the mobility of spin labels. This behavior is consistent with previous studies on telodendrimer-based NPs having polyethylene glycol (PEG) in the surface.³⁵ The same study by Li *et al.* has also demonstrated that lipoprotein particles, particularly LDL can interact with the non-cross-linked NPs composed of a PEG shell and disrupt their assembly structure rapidly. It was proposed that lipoprotein particles and micellar NPs are likely to exchange contents with each other due to the similar amphiphilic nature causing the disassembly of the NPs.³⁵ To overcome this effect the NPs were additionally stabilized by introducing disulfide cross-links within the core.⁵⁸ Such micelles exhibit superior structural stability compared to their non-cross-linked counterparts^{64–66} and can better retain their assembly structure in the presence of blood proteins.³⁵ However, to release the drug payload the intra-micellar disulfide bonds should first be cleaved by a reducing agent, which could be inconvenient in some therapeutic cases. Contrarily, we found that the shape of the EPR spectra and calculated correlation times remained unchanged after incubation of RNP-Ss and RNP-C in LDL and HDL compared to the spectra in PBS (Fig. 6, Tables S4 and S5). These results indicate that the lipoproteins (HDL and LDL) are not able to bind or penetrate the hydrophilic shell of NPs such as RNP-Ss and RNP-C and the micelles could retain their structural integrity even without additional crosslinking. This can be explained by the unique structure of HPMA copolymers. In contrast with PEG, HPMA has lower propensity

to form hydrogen bonds and therefore no interactions are possible between HPMA copolymer shell and proteins and lipoproteins. Cukalevski *et al.* recently found that immunoglobulin G (IgG), the main type of antibody found in blood, enhance the aggregation of polystyrene NPs by forming protein bridges between them.⁶⁷ Our EPR results, however, show that even if the bridges are formed at the surface of HPMA copolymer based NPs they do not make strong enough connections with HPMA polymer chains to influence their mobility (Fig. 6(b), Table S5). Finally, we investigated how the human plasma influence chain dynamics in HPMA copolymer based NPs. Again, it can be seen (Fig. 6, Table S4 and S5) that the mobility of the spin labels in RNP-C and RNP-Ss was not affected by human plasma. This finding is in contrast with previously published results on PEG based NPs whose assembly order was immediately lost after incubation in human plasma as reflected in the sharper EPR spectrum.³⁵

To verify the conclusions obtained from our EPR studies, two complimentary methods were exploited. Since HSA is the most abundant protein in blood plasma, ITC experiments were performed to check its binding affinity to RNP-C and RNP-Ss NPs. A blank experiment with titration of HSA solution into PBS buffer shows endothermic peaks whose amplitude decreases with increasing of HSA concentration in solution (Fig. 7(a)). Such behavior is usually observed for dilution experiments of polymers and proteins. Titration of HSA into RNP-C and RNP-Ss shows only minor changes in comparison with the blank experiment (Fig. 7(b)). There is no strong adsorption of HSA on nanoparticle surface which is in agreement with EPR results presented above. The small mismatch between curves could be attributed to insignificant interactions of HSA with polymers resulting in formation of the thin layer of HSA that exists in dynamic equilibrium with polymer chains.

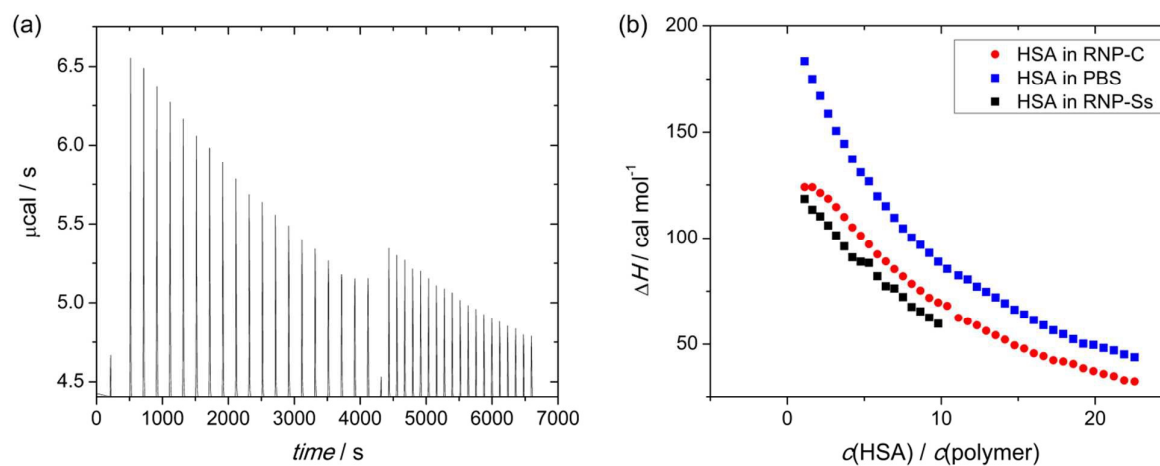


Fig. 7 ITC experiments: (a) the heat flow per injection in titration of HSA ($c = 50 \text{ mg} \cdot \text{mL}^{-1}$ in PBS) into PBS buffer. (b) Observed enthalpy changes for the titration of HSA ($c = 50 \text{ mg} \cdot \text{mL}^{-1}$) into RNP-C ($1 \text{ mg} \cdot \text{mL}^{-1}$ in PBS) and RNP-Ss ($1 \text{ mg} \cdot \text{mL}^{-1}$ in PBS). $T = 37^\circ\text{C}$

One might expect that the presence of a thick corona could be recognized by the distribution function of R_h in DLS experiments since larger objects, with scattered intensity proportional to the sixth power of size, scatter more

effectively than small entities. Closer inspection of distribution functions shows no significant difference between the distribution functions of each particular protein and the solution in the presence of polymer NPs (Figs. 8(a) and (b)).

We explain these findings by the presence of large protein aggregates that suppress the scattering from NPs. Such

conclusion is in agreement with Cryo-TEM results (Figs. S3-S6), where polydisperse aggregates are clearly visible.

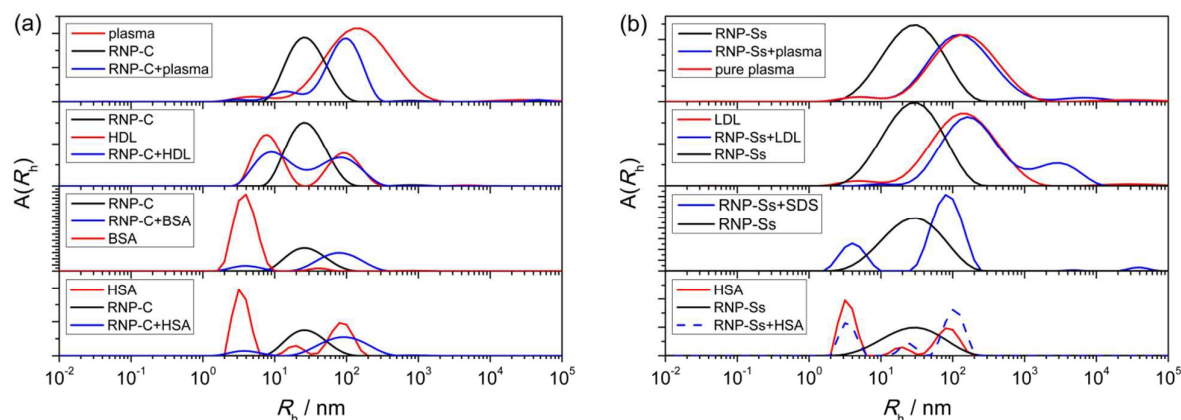


Fig. 8 Distribution functions $A(R_h)$ for (a) RNP-C and (b) RNP-Ss in the presence of different proteins. The distribution functions of pure proteins and pure NPs in solution are presented for comparison.

With these results from EPR, ITC, and DLS methods it is possible to conclude that blood plasma proteins form no hard corona around HPMA based NPs. This result is in perfect agreement with *in vivo* testing of drug carriers based on amphiphilic HPMA polymer conjugates with doxorubicin.³⁷ Indeed, HPMA copolymers provide perfect “stealth” properties to NPs preventing them from interaction with human blood plasma proteins and, thus, keeping their functionality unchanged. All previous publications where “hard corona-soft corona” was reported should be reevaluated now with respect to the type of NPs that have been used to study protein adsorption. In contrast with HPMA copolymers systems, all previous publications cluster around NPs with strong either hydrophobic, or charged surface. Even the presence of PEG as a shell results in the formation of protein corona due to hydrogen bond interactions.

Conclusions

The presence of protein corona around biocompatible HPMA copolymer-based NPs was inspected by a method with the highest sensitivity to polymer chain dynamics - electron paramagnetic resonance (EPR). In contrast to previous observations, no “hard corona-soft corona” structure was observed for radical containing NPs (RNP) differing in the location of TEMPO radical in the NP structure in the presence of HSA, IgG, low- and high-density lipoproteins, and human blood plasma itself. Our study confirms that a classical “hard corona-soft corona” paradigm is not valid for all types of NPs and each system has unique protein corona that is determined by the nature of NP material.

Acknowledgments

We acknowledge financial support from the Ministry of Education, Youth and Sports of the Czech Republic, grant No. LH15213. This work was supported by the grants 17-07164S from the Czech Science Foundation and the Progres Q28 from Charles University. The authors thank to Dr. O. Janouskova (Institute of Macromolecular Chemistry, Academy of Sciences of the Czech Republic) for providing blood plasma.

Notes and references

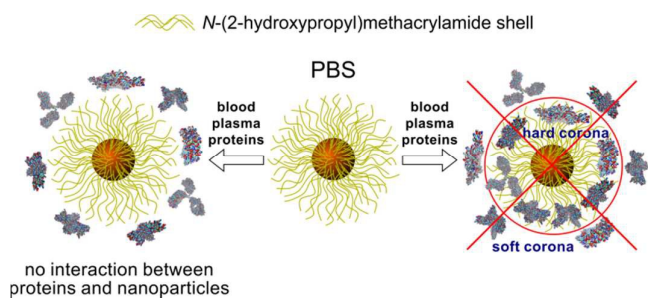
- 1 E. Blanco, H. Shen and M. Ferrari, *Nat. Biotechnol.*, 2015, **33**, 941–951.
- 2 A. M. Jhaveri and V. P. Torchilin, *Front. Pharmacol.*, 2014, **5**, 1–26.
- 3 C. J. Cheng, G. T. Tietjen, J. K. Saucier-Sawyer and W. M. Saltzman, *Nat. Rev. Drug Discov.*, 2015, **14**, 239–247.
- 4 N. Kamaly, Z. Xiao, P. M. Valencia, A. F. Radovic-Moreno and O. C. Farokhzad, *Chem. Soc. Rev.*, 2012, **41**, 2971–3010.
- 5 P. Aggarwal, J. B. Hall, C. B. McLeland, M. A. Dobrovolskaia and S. E. McNeil, *Adv. Drug Deliv. Rev.*, 2009, **61**, 428–437.
- 6 T. Cedervall, I. Lynch, S. Lindman, T. Berggård, E. Thulin, H. Nilsson, K. A. Dawson and S. Linse, *Proc. Natl. Acad. Sci.*, 2007, **104**, 2050–2055.
- 7 M. Mahmoudi, I. Lynch, M. R. Ejtehadi, M. P. Monopoli, F. B. Bombelli and S. Laurent, *Chem. Rev.*, 2011, **111**, 5610–5637.
- 8 Y. Kim, S. M. Ko and J.-M. Nam, *Chem. – Asian J.*, 2016, **11**, 1869–1877.
- 9 S. R. Saptarshi, A. Duschl and A. L. Lopata, *J. Nanobiotechnology*, 2013, **11**, 26.
- 10 A. A. Shemetov, I. Nabiev and A. Sukhanova, *ACS Nano*, 2012, **6**, 4585–4602.

- 11 M. Rahman, S. Laurent, N. Tawil, L. Yahia and M. Mahmoudi, *Protein-Nanoparticle Interactions: The Bio-Nano Interface*, Springer, Heidelberg ; New York, 2013.
- 12 S.-T. Yang, Y. Liu, Y.-W. Wang and A. Cao, *Small*, 2013, **9**, 1635–1653.
- 13 C. D. Walkey and W. C. W. Chan, *Chem. Soc. Rev.*, 2012, **41**, 2780–2799.
- 14 M. P. Monopoli, C. Åberg, A. Salvati and K. A. Dawson, *Nat. Nanotechnol.*, 2012, **7**, 779–786.
- 15 M. Lundqvist, J. Stigler, T. Cedervall, T. Berggård, M. B. Flanagan, I. Lynch, G. Elia and K. Dawson, *ACS Nano*, 2011, **5**, 7503–7509.
- 16 I. Lynch and K. A. Dawson, *Nano Today*, 2008, **3**, 40–47.
- 17 P. P. Karmali and D. Simberg, *Expert Opin. Drug Deliv.*, 2011, **8**, 343–357.
- 18 Y. K. Lee, E.-J. Choi, T. J. Webster, S.-H. Kim and D. Khang, *Int. J. Nanomedicine*, 2015, **10**, 97–113.
- 19 D. Walczyk, F. B. Bombelli, M. P. Monopoli, I. Lynch and K. A. Dawson, *J. Am. Chem. Soc.*, 2010, **132**, 5761–5768.
- 20 L. Vroman and A. L. Adams, *J. Colloid Interface Sci.*, 1986, **111**, 391–402.
- 21 Z. Zhu, C. Xie, Q. Liu, X. Zhen, X. Zheng, W. Wu, R. Li, Y. Ding, X. Jiang and B. Liu, *Biomaterials*, 2011, **32**, 9525–9535.
- 22 S. Kamei and J. Kopeček, *Pharm. Res.*, 1995, **12**, 663–668.
- 23 D. F. Moyano, K. Saha, G. Prakash, B. Yan, H. Kong, M. Yazdani and V. M. Rotello, *ACS Nano*, 2014, **8**, 6748–6755.
- 24 C. Pinholt, J. T. Bukrinsky, S. Hostrup, S. Frokjaer, W. Norde and L. Jorgensen, *Eur. J. Pharm. Biopharm.*, 2011, **77**, 139–147.
- 25 L. Li, Q. Mu, B. Zhang and B. Yan, *Analyst*, 2010, **135**, 1519–1530.
- 26 N. Li, S. Zeng, L. He and W. Zhong, *Anal. Chem.*, 2010, **82**, 7460–7466.
- 27 D. Bartczak, P. Vincent and H. Goenaga-Infante, *Anal. Chem.*, 2015, **87**, 5482–5485.
- 28 M. Hemmelmann, K. Mohr, K. Fischer, R. Zentel and M. Schmidt, *Mol. Pharm.*, 2013, **10**, 3769–3775.
- 29 K. Mohr, S. S. Müller, L. K. Müller, K. Rusitzka, S. Gietzen, H. Frey and M. Schmidt, *Langmuir*, 2014, **30**, 14954–14962.
- 30 L. Nuhn, S. Gietzen, K. Mohr, K. Fischer, K. Toh, K. Miyata, Y. Matsumoto, K. Kataoka, M. Schmidt and R. Zentel, *Biomacromolecules*, 2014, **15**, 1526–1533.
- 31 S. Winzen, S. Schoettler, G. Baier, C. Rosenauer, V. Mailaender, K. Landfester and K. Mohr, *Nanoscale*, 2015, **7**, 2992–3001.
- 32 C. D. Walkey, J. B. Olsen, F. Song, R. Liu, H. Guo, D. W. H. Olsen, Y. Cohen, A. Emili and W. C. W. Chan, *ACS Nano*, 2014, **8**, 2439–2455.
- 33 L. J. Berliner and J. Reuben, Eds., *Spin Labeling*, Springer US, Boston, MA, 1989, vol. 8.
- 34 S. Valić, M. Andreis and D. Klepac, in *Handbook of Multiphase Polymer Systems*, eds. A. Boudenne, L. Ibos, Y. Candau and S. Thomas, John Wiley & Sons, Ltd, Chichester, UK, 2011, pp. 551–584.
- 35 Y. Li, M. S. Budamagunta, J. Luo, W. Xiao, J. C. Voss and K. S. Lam, *ACS Nano*, 2012, **6**, 9485–9495.
- 36 S. Petrova, D. Klepac, R. Konefař, S. Kereřice, L. Kováčik and S. K. Filippov, *Macromolecules*, 2016, **49**, 5407–5417.
- 37 P. Chytil, T. Etrych, Č. Koňák, M. Šírová, T. Mrkvan, J. Bouček, B. Říhová and K. Ulbrich, *J. Controlled Release*, 2008, **127**, 121–130.
- 38 S. K. Filippov, P. Chytil, P. V. Konarev, M. Dyakonova, C. Papadakis, A. Zhigunov, J. Plestil, P. Stepanek, T. Etrych, K. Ulbrich and D. I. Svergun, *Biomacromolecules*, 2012, **13**, 2594–2604.
- 39 K. Ulbrich, V. Šubr, J. Strohalm, D. Plocová, M. Jelínková and B. Říhová, *J. Controlled Release*, 2000, **64**, 63–79.
- 40 V. Šubr and K. Ulbrich, *React. Funct. Polym.*, 2006, **66**, 1525–1538.
- 41 T. Etrych, T. Mrkvan, P. Chytil, Č. Koňák, B. Říhová and K. Ulbrich, *J. Appl. Polym. Sci.*, 2008, **109**, 3050–3061.
- 42 E. Lepeltier, C. Bourgaux and P. Couvreur, *Adv. Drug Deliv. Rev.*, 2014, **71**, 86–97.
- 43 D. E. Budil, S. Lee, S. Saxena and J. H. Freed, *J. Magn. Reson. A*, 1996, **120**, 155–189.
- 44 J. Dubochet, M. Adrian, J.-J. Chang, J.-C. Homo, J. Lepault, A. W. McDowell and P. Schultz, *Q. Rev. Biophys.*, 1988, **21**, 129–228.
- 45 S. Schlick, Ed., *Advanced ESR Methods in Polymer Research*, John Wiley & Sons, Inc., Hoboken, NJ, USA, 2006.
- 46 Z. Vekslí, M. Andreis and B. Rakvin, *Prog. Polym. Sci.*, 2000, **25**, 949–986.
- 47 M. Drescher and G. Jeschke, Eds., *EPR Spectroscopy: Applications in Chemistry and Biology*, Springer, Heidelberg, 2012.
- 48 S. Domingo Köhler, A. Weber, S. P. Howard, W. Welte and M. Drescher, *Protein Sci.*, 2010, **19**, 625–630.
- 49 J. Pilar, J. Labsky, J. Kalal and J. H. Freed, *J. Phys. Chem.*, 1979, **83**, 1907–1914.
- 50 A. K. Bhuyan, *Biopolymers*, 2010, **93**, 186–199.
- 51 N. Kang, M.-È. Perron, R. E. Prud'homme, Y. Zhang, G. Gaucher and J.-C. Leroux, *Nano Lett.*, 2005, **5**, 315–319.
- 52 J. V. M. Weaver, Y. Tang, S. Liu, P. D. Iddon, R. Grigg, N. C. Billingham, S. P. Armes, R. Hunter and S. P. Rannard, *Angew. Chem. Int. Ed.*, 2004, **43**, 1389–1392.
- 53 C. Yang, J. P. K. Tan, W. Cheng, A. B. E. Attia, C. T. Y. Ting, A. Nelson, J. L. Hedrick and Y.-Y. Yang, *Nano Today*, 2010, **5**, 515–523.
- 54 M. J. Joralemon, R. K. O'Reilly, C. J. Hawker and K. L. Wooley, *J. Am. Chem. Soc.*, 2005, **127**, 16892–16899.
- 55 E. S. Read and S. P. Armes, *Chem. Commun.*, 2007, **0**, 3021–3035.
- 56 M. Elsalaby and K. L. Wooley, *Chem. Soc. Rev.*, 2012, **41**, 2545–2561.
- 57 A. N. Koo, H. J. Lee, S. E. Kim, J. H. Chang, C. Park, C. Kim, J. H. Park and S. C. Lee, *Chem. Commun.*, 2008, **0**, 6570–6572.
- 58 Y. Li, K. Xiao, J. Luo, W. Xiao, J. S. Lee, A. M. Gonik, J. Kato, T. A. Dong and K. S. Lam, *Biomaterials*, 2011, **32**, 6633–6645.
- 59 N. L. Anderson and N. G. Anderson, *Mol. Cell. Proteomics*, 2002, **1**, 845–867.
- 60 S. Lewington, G. Whitlock, R. Clarke, P. Sherliker, J. Emberson, J. Halsey, N. Qizilbash, R. Peto and R. Collins, *The Lancet*, 2007, **370**, 1829–1839.
- 61 A. Gonzalez-Quintela, R. Alende, F. Gude, J. Campos, J. Rey, L. M. Meijide, C. Fernandez-Merino and C. Vidal, *Clin. Exp. Immunol.*, 2008, **151**, 42–50.
- 62 G. Fanali, A. di Masi, V. Trezza, M. Marino, M. Fasano and P. Ascenzi, *Mol. Aspects Med.*, 2012, **33**, 209–290.
- 63 B. A. Aguilar-Castillo, J. L. Santos, H. Luo, Y. E. Aguirre-Chagala, T. Palacios-Hernández and M. Herrera-Alonso, *Soft Matter*, 2015, **11**, 7296–7307.
- 64 H. Wei, R.-X. Zhuo and X.-Z. Zhang, *Prog. Polym. Sci.*, 2013, **38**, 503–535.
- 65 Y. Li, K. Xiao, W. Zhu, W. Deng and K. S. Lam, *Adv. Drug Deliv. Rev.*, 2014, **66**, 58–73.
- 66 K. Xiao, Y.-P. Li, C. Wang, S. Ahmad, M. Vu, K. Kuma, Y.-Q. Cheng and K. S. Lam, *Biomaterials*, 2015, **67**, 183–193.

ARTICLE

Journal Name

- 67 R. Cukalevski, S. A. Ferreira, C. J. Dunning, T. Berggård and T. Cedervall, *Nano Res.*, 2015, **8**, 2733–2743.



Classical “hard corona-soft corona” paradigm is not valid for HPMA-based nanoparticles.